Modeling of hydrogen storage in hydride-forming materials: Equilibrium gas-phase kinetics

A. Ledovskikh,[1] D. Danilov,[2] and P. H. L. Notten[1,3,*]
[1]*Eindhoven University of Technology, Den Dolech 2, 5600 MB Eindhoven, The Netherlands*
[2]*Eurandom, Den Dolech 2, 5600 MB Eindhoven, The Netherlands*
[3]*Philips Research Laboratories, High Tech Campus 4, 5656 AE Eindhoven, The Netherlands*
(Received 5 February 2007; revised manuscript received 18 April 2007; published 13 August 2007)

A kinetic model has been developed, describing the kinetics of the hydrogen storage reactions in hydride-forming materials under equilibrium conditions. Based on first principles chemical reaction kinetics and statistical thermodynamics, the model is able to describe the complex processes occurring in hydrogen storage systems, including phase transitions. A complete set of equations, governing pressure-composition isotherms in both solid-solution and two-phase coexistence regions has been obtained. General expressions for rate constant dependencies have been proposed, using well-defined phase-dependent Hamiltonians for the hydrogen energy state at the surface and in the bulk of hydride-forming materials. The characteristics of both model ($LaNi_yCu_{1.0}$) and commercial, misch-metal-based AB_5-type materials at different compositions and temperatures have been simulated. Good agreement between experimental and theoretical results for the pressure-composition isotherms has been found in all cases.

DOI: 10.1103/PhysRevB.76.064106 PACS number(s): 64.60.−i, 05.50.+q, 05.70.−a, 82.20.−w

I. INTRODUCTION

Modern society urgently needs clean, renewable, and efficient energy storage devices. Sustainable energy suppliers are promoting a sustainable economic development and are improving the quality of life by protecting the environment. It is generally expected that hydrogen will play an important role in such sustainable society. Hydrogen storage is, however, considered to be one of the limiting factors in the future hydrogen economy.

Metal-hydride (MH) compounds are successfully employed as efficient hydrogen storage media via the gas phase. This is one of the key factors, enabling the use of hydrogen-driven fuel cells. A second, electrochemical, application of MH materials is in high energy density, nickel metal-hydride batteries, nowadays widely applied in many portable electronics and hybrid electrical vehicles.[1–6]

Hydrogen storage via the gas phase is a highly complex multistage process. The first step in the storage process is dissociation of hydrogen molecules at the interface between the metal and the gas phase. This represents the adsorption process. The adsorbed hydrogen atoms can then penetrate into the MH material and occupy the available interstitial sites, inducing hydrogen absorption. The absorbed hydrogen atoms are transported inside the bulk of the hydride-forming material by conventional diffusion. Evidently, chemical equilibrium exists between hydrogen stored in the solid and that present in the gas phase, which is generally characterized by pressure-composition isotherms.[3–7]

A typical pressure-composition absorption isotherm and accompanying phase diagram are schematically shown in curves (a) and (b) of Fig. 1, respectively.[7–11] During hydrogen absorption at low concentrations, a solid solution is formed, which is generally denoted as the α phase. In this concentration region the partial hydrogen pressure ($P_{H_2}^{eq}$) is clearly dependent on the amount of stored hydrogen. After the hydrogen concentration has reached a certain critical value (x_α), phase transition occurs and the α phase is continuously transformed into the β phase. The pressure dependence in this two-phase coexistence region is generally characterized by a (sloping) plateau.[7,12] Phase transition is completed at x_β and a solid solution is subsequently formed by the β phase only. This typical three-step process will play an important role in the subsequent part of this paper.

Recently a statistical lattice gas model (LGM) has been proposed by the present authors.[13] This model is based on first principles of statistical thermodynamics and takes into account the hydrogen absorption and desorption in hydride-forming materials in both solid-solution and two-phase coexistence regions. However, the LGM only describes the thermodynamics of these processes. No kinetic considerations are included. The advantage of the kinetic approach is that it can describe both the equilibrium and dynamic (nonequilibrium) conditions. In this contribution, however, only the reaction kinetics under equilibrium conditions will be considered. In a forthcoming paper the dynamic model will be presented in detail.

There are a number of papers discussing the various aspects of the hydrogen absorption/desorption kinetics. Martin *et al.*[14] proposed a detailed reaction scheme but did not address the equilibrium situation. Fernandez *et al.*[15] and Feldman *et al.*[16] suffer from similar drawbacks. To the best of our knowledge only a few attempts have been made to describe equilibrium kinetics of complex systems. One of the first and very fundamental work is that of Gileadi,[17,18] describing the kinetics to determine the rate constant dependencies on the surface coverage of the species involved and adopting Langmuir- and Temkin-type approaches. However, the considered system is different from the present MH-storage system and some kinetic equations are rather empirical of nature.[17,18] The first attempt to describe a complete hydrogen storage system from a kinetic point-of-view was made by Feng *et al.*[19] The authors applied the equilibrium kinetics approach to describe pressure-composition isotherms and obtained good agreement with experimental data. However, their description of phase transition and hydrogen surface

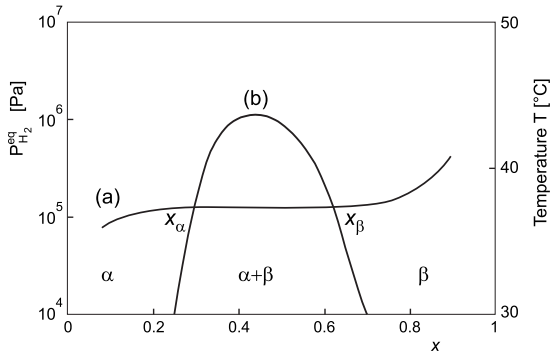

FIG. 1. Schematic representation of a pressure-composition isotherm (a) and phase diagram (b) for a typical hydrogen storage material. The α and β solid-solution regions are indicated together with the temperature-dependent two-phase ($\alpha+\beta$) miscibility gap.

recombination are oversimplified and rate constant expressions are again empirical of nature.

In the present paper, an equilibrium kinetic model is proposed. This model is based on first principles of chemical reaction kinetics and statistical thermodynamics and takes into account hydrogen dissociation/recombination and absorption/desorption at/in hydride-forming materials in both the solid-solution and two-phase coexistence regions. A general and systematic approach to determine activation energies and rate constants will be provided. The simulated hydrogen pressure-composition isotherms will be compared with a wide variety of experimental results, revealing very good agreement in all cases.

II. MODEL

A. System description

The hydrogen absorption process via the gas phase is considered in more detail in Fig. 2. After dissociation at the metal surface (M^s) the hydrogen atoms are chemically adsorbed (H_{ad}) and then converted to the absorbed state (H_{abs}) in the first atomic layer, which has been denoted as the sublayer or subsurface.[8] Subsequently, hydrogen is transported into the bulk of the material (M^b) by conventional diffusion. In Fig. 2, x represents the normalized hydrogen concentration in the bulk of the hydride-forming material, θ is the normalized surface coverage, and c_g is the hydrogen concentration in the gas phase. Essentially, two reaction steps must at least be considered to describe the absorption/desorption process: the hydrogen dissociation/recombination reaction at the solid/gas interface

$$2M^s + H_2 \underset{k_{-1}}{\overset{k_1}{\rightleftarrows}} 2M^sH_{ad} \tag{1}$$

and hydrogen absorption/desorption in the bulk, according to

$$M^b + M^sH_{ad} \underset{k_{-2}}{\overset{k_2}{\rightleftarrows}} M^bH_{abs} + M^s. \tag{2}$$

The general reactions described by Eqs. (1) and (2) are considered to take place separately at and within each phase.

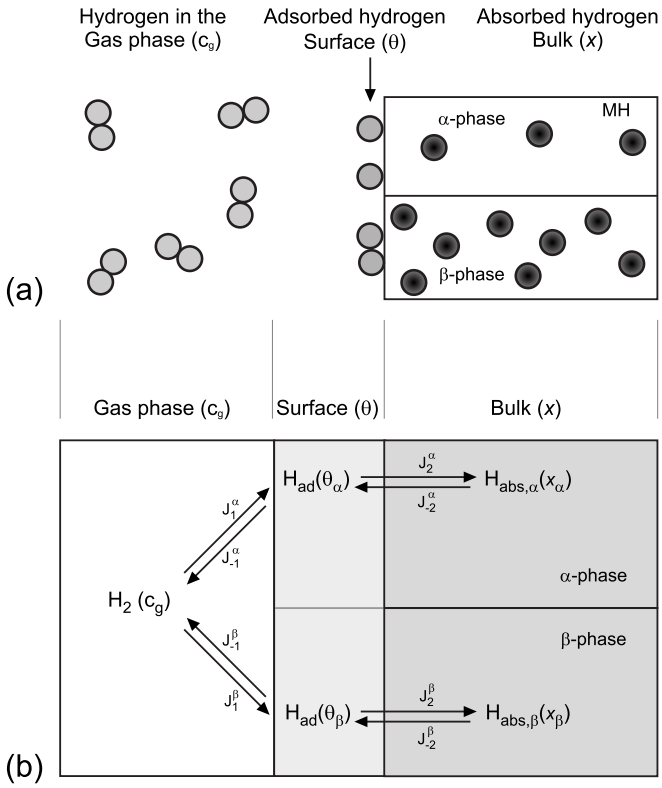

FIG. 2. (a) Schematic representation of the hydrogen storage process. (b) General (de)hydrogenation reaction scheme, including the dissociation and recombination reaction at the surface and the hydrogen absorption and desorption in the bulk of the hydride-forming material.

Consequently, this also holds for the reaction flows, which are assumed to occur at/in each phase independently, as is schematically indicated in Fig. 2(b). From Fig. 2 it is clear that hydrogen plays an important role at three distinct areas, in the bulk of the material, at the solid/gas interface, and in the gas phase. The system will therefore be defined in line with these distinct phases.

B. System definition

1. Bulk

Assuming that the bulk of the hydrogen storage material consists of M unit cells, which can be either in the α (M_α) or β state (M_β), this leads to

$$M = M_\alpha + M_\beta. \tag{3}$$

When the crystallographic structure of both phases is assumed to be identical, as is the case for many hydride-forming compounds, M remains constant throughout the hydrogenation process. It is furthermore assumed that the number of host sites per unit cell in both the α and β phase is equal. This number is denoted as d^b. The total number of host sites in the bulk (N^b) can be obtained from

$$N^b = N^b_\alpha + N^b_\beta = d^bM_\alpha + d^bM_\beta. \tag{4}$$

The number of hydrogen guest atoms in the α and β phase is denoted by n_α^b and n_β^b, respectively, where the total number of occupied hydrogen sites (n^b) is given by the summation of n_α^b and n_β^b.[13] When $n_{\max}^b$ represents the maximal number of host sites in the bulk that can be occupied by hydrogen, the normalized number of absorbed hydrogen atoms x in the system can then be represented by

$$x = \frac{n^b}{n_{\max}^b} = \frac{n_\alpha^b + n_\beta^b}{n_{\max}^b}, \tag{5}$$

in which the partial hydrogen concentrations in each phase (i) are defined as

$$x^i = \frac{n_i^b}{n_{\max}^b}. \tag{6}$$

Curves (a) and (b) in Fig. 3(a) show the normalized number of host sites $N_i^b/n_{\max}^b$ as a function of the normalized hydrogen content in the α and β phase, respectively. The dependence of N_α^b and N_β^b on x in the three crystallographic regions can mathematically be represented by

$$N_\alpha^b = \begin{cases} d^b M, & x < \mathrm{x}_\alpha, \\ d^b M\left(\dfrac{\mathrm{x}_\beta - x}{\mathrm{x}_\beta - \mathrm{x}_\alpha}\right), & \mathrm{x}_\alpha \le x \le \mathrm{x}_\beta, \\ 0, & x > \mathrm{x}_\beta, \end{cases}$$

$$N_\beta^b = \begin{cases} 0, & x < \mathrm{x}_\alpha, \\ d^b M\left(\dfrac{x - \mathrm{x}_\alpha}{\mathrm{x}_\beta - \mathrm{x}_\alpha}\right), & \mathrm{x}_\alpha \le x \le \mathrm{x}_\beta, \\ d^b M, & x > \mathrm{x}_\beta. \end{cases} \tag{7}$$

In Fig. 3(b) [curves (a) and (b)] the development of the partial hydrogen concentrations ($n_i^b/n_{\max}^b$) is shown. At low hydrogen concentration the hydrogen atoms fill the available α sites only. The maximum concentration level within the α phase is reached at $x=\mathrm{x}_\alpha$. Here, phase transition is initiated and n_α^b decreases linearly in the two-phase coexistence region. Finally n_α^b becomes zero when phase transition is completed at x_β. It is assumed that all available host sites are fully occupied by hydrogen atoms at $x=1$, i.e., when $n_\beta^b = N_\beta^b = n_{\max}^b$. The following mathematical expressions reveal the dependence of n_α^b and n_β^b on x:

$$n_\alpha^b = \begin{cases} x n_{\max}^b, & x < \mathrm{x}_\alpha, \\ \mathrm{x}_\alpha n_{\max}^b\left(\dfrac{\mathrm{x}_\beta - x}{\mathrm{x}_\beta - \mathrm{x}_\alpha}\right), & \mathrm{x}_\alpha \le x \le \mathrm{x}_\beta, \\ 0, & x > \mathrm{x}_\beta, \end{cases}$$

$$n_\beta^b = \begin{cases} 0, & x < \mathrm{x}_\alpha, \\ \mathrm{x}_\beta n_{\max}^b\left(\dfrac{x - \mathrm{x}_\alpha}{\mathrm{x}_\beta - \mathrm{x}_\alpha}\right), & \mathrm{x}_\alpha \le x \le \mathrm{x}_\beta, \\ x n_{\max}^b, & x > \mathrm{x}_\beta. \end{cases} \tag{8}$$

As will become clear later, it is also convenient to define the phase-normalized hydrogen concentrations, for which normalization takes place with respect to the available host sites within each individual phase (N_i^b), according to

$$x_i = \frac{n_i^b}{N_i^b}. \tag{9}$$

Obviously, as Fig. 3(c) reveals, the phase-normalized concentrations remain constant in the two-phase coexistence region for both phases. It is evident that $x \neq x_\alpha + x_\beta$ while, on the other hand, $x = x^\alpha + x^\beta$ [see Fig. 3(b)].

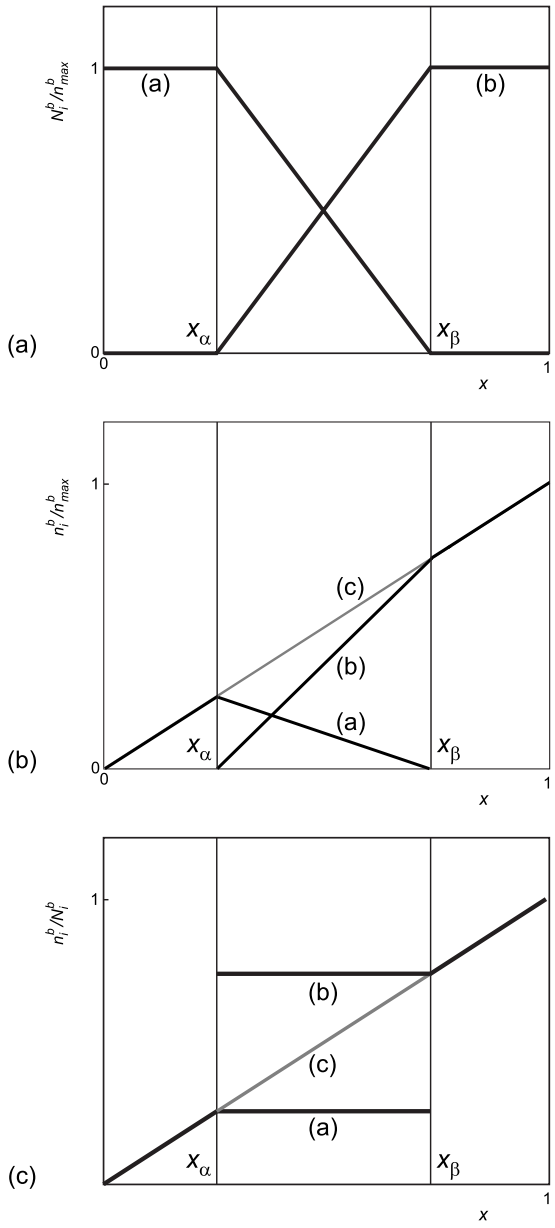

FIG. 3. Normalized number of host sites ($N_i^b/n_{\max}^b$) as a function of normalized hydrogen concentration (x) in the α [curve (a)] and β phase [curve (b)]. (b) Partial hydrogen concentrations [$x^i = n_i^b/n_{\max}^b$, see Eq. (6)] as a function of x in the same two phases; curve (c) is the total hydrogen concentration. (c) Phase-normalized hydrogen concentrations [$x_i = n_i^b/N_i^b$, see Eq. (9)] as a function of x.

2. Surface

Similar to the bulk, the number of the host sites and guest hydrogen atoms can be defined by N_i^s and n_i^s, respectively, and the normalized surface coverage θ is defined as

$$\theta = \frac{n^s}{n^s_{\max}} = \frac{n^s_\alpha + n^s_\beta}{n^s_{\max}}, \tag{10}$$

where $n^s_{\max}$ is the maximal number of host sites at the surface that can be occupied by hydrogen. The partial surface coverage can for each phase (θ^α and θ^β) be represented by

$$\theta^i = \frac{n^s_i}{n^s_{\max}}. \tag{11}$$

On the analogy of the bulk, the phase-normalized surface coverage is defined as

$$\theta_i = \frac{n^s_i}{N^s_i}. \tag{12}$$

In order to describe the kinetics of the various reaction steps properly, the surface area of each individual phase is required. Denoting the surface area of the hydride-forming material occupied by a particular phase as A_i and assuming that the fraction of each phase at the surface is proportional to the amount of that particular phase present in the bulk, the following expression is obtained:

$$A_i = A_0 \frac{N^b_i}{n^b_{\max}}, \tag{13}$$

in which A_0 is the total surface area of the system. For simplicity, it is assumed that the total surface area remains constant throughout the (de)hydrogenation process, which is generally to be the case after material activation has been completed.[3] Furthermore, volumetric changes caused by the (de)hydrogenation process are neglected.

3. Gas phase

The general gas law is adopted for the gas phase, relating the partial hydrogen pressure ($P^{\text{eq}}_{\text{H}_2}$) and the concentration of hydrogen in the gas phase (c_g) at a given temperature (T), according to

$$P^{\text{eq}}_{\text{H}_2} = RTc_g. \tag{14}$$

C. Reaction kinetics

From Fig. 2 it is clear that two reaction steps [Eqs. (1) and (2)] have to be taken into account at each individual phase. Considering the basic principles of reaction kinetics the dissociation (J^i_1) and recombination (J^i_{-1}) fluxes [mol/s] can, for each phase i in the total system be described by

$$\begin{cases} J^i_1 = \bar{k}^i_1 A_i [c^s_i(M)]^2 c_g, \\ J^i_{-1} = \bar{k}^i_{-1} A_i [c^s_i(MH)]^2, \end{cases} \quad i = \alpha, \beta, \tag{15}$$

where $\bar{k}^i_1$ [$\text{m}^5\ \text{mol}^{-2}\ \text{s}^{-1}$] is the dissociation rate constant, $\bar{k}^i_{-1}$ [$\text{m}^2\ \text{mol}^{-1}\ \text{s}^{-1}$] the recombination rate constant, A_i [m^2] the surface area of phase i, $c^s_i(M)$ [$\text{mol}\ \text{m}^{-2}$] the surface concentration of nonoccupied host sites, $c^s_i(MH)$ [$\text{mol}\ \text{m}^{-2}$] the surface concentration of occupied host sites and c_g is given in [$\text{mol}\ \text{m}^{-3}$]. It is worthwhile to note that in this work concentrations are used instead of activities, i.e., all activity coefficients are considered unity.

The surface concentrations $c^s_i(M)$ and $c^s_i(MH)$ in Eq. (15) can be expressed in terms of the number of host sites, guest hydrogen atoms, and phase-normalized surface coverage [Eq. (12)] as

$$\begin{cases} c^s_i(M) = \dfrac{N^s_i - n^s_i}{N_A A_i} = (1-\theta_i)\dfrac{N^s_i}{N_A A_i}, \\ c^s_i(MH) = \dfrac{n^s_i}{N_A A_i} = \theta_i \dfrac{N^s_i}{N_A A_i}, \end{cases} \tag{16}$$

where N_A is Avogadro's number and $N^s_i/N_A A_i$ is a material constant, representing the available host sites per unit area [$\text{mol}\ \text{m}^{-2}$]. As volume expansion upon hydrogenation is neglected in this work, this constant is the same for both phases. Replacing these concentrations in Eq. (15) together with the expressions for A_i [Eq. (13)] and c_g [Eq. (14)], and dividing the obtained fluxes [Eq. (15)] by the total surface area of the system (A_0), normalized fluxes are obtained for the dissociation (j^i_1) and recombination (j^i_{-1}) reactions [$\text{mol}\ \text{m}^{-2}\ \text{s}^{-1}$], according to

$$\begin{cases} j^i_1 = k^i_1 (1-\theta_i)^2 \dfrac{N^b_i P_{\text{H}_2}}{n^b_{\max} RT}, \\ j^i_{-1} = k^i_{-1} \theta_i^2 (N^b_i / n^b_{\max}), \end{cases} \tag{17}$$

where $k^i_1 = \bar{k}^i_{-1} \left(\dfrac{N^s_i}{N_A A_i} \right)^2$ is the redefined dissociation rate constant [$\text{mol}\ \text{m}^{-2}\ \text{s}^{-1}$] and $k^i_{-1} = \bar{k}^i_{-1} \left(\dfrac{N^s_i}{N_A A_i} \right)^2$ is the redefined recombination rate constant [$\text{mol}\ \text{m}^{-2}\ \text{s}^{-1}$].

In equilibrium, the fluxes of the forward and backward reactions are exactly balanced, leading to the following expressions in the three defined crystallographic regions

$$\begin{cases} j^\alpha_1 = j^\alpha_{-1}, & 0 \le x < \text{x}_\alpha, \\ j^\alpha_1 + j^\beta_1 = j^\alpha_{-1} + j^\beta_{-1}, & \text{x}_\alpha \le x \le \text{x}_\beta, \\ j^\beta_1 = j^\beta_{-1}, & \text{x}_\beta < x \le 1. \end{cases} \tag{18}$$

Introducing the normalized reaction fluxes [Eq. (17)] into Eq. (18), the analytical solution is obtained which expresses the equilibrium hydrogen pressure in the three distinct regions, according to

$$P_{H_2}^{eq} = RT \begin{cases} \left(\frac{\theta}{1-\theta}\right)^2 \frac{k_{-1}^{\alpha}}{k_1^{\alpha}}, & 0 \le x < x_{\alpha}, \\ \frac{k_{-1}^{\alpha}(\theta_{\alpha})^2 (N_{\alpha}^b / n_{\max}^b) + k_{-1}^{\beta}(\theta_{\beta})^2 (N_{\beta}^b / n_{\max}^b)}{k_1^{\alpha}(1-\theta_{\alpha})^2 (N_{\alpha}^b / n_{\max}^b) + k_1^{\beta}(1-\theta_{\beta})^2 (N_{\beta}^b / n_{\max}^b)}, & x_{\alpha} \le x \le x_{\beta}, \\ \left(\frac{\theta}{1-\theta}\right)^2 \frac{k_{-1}^{\beta}}{k_1^{\beta}}, & x_{\beta} < x \le 1. \end{cases} \tag{19}$$

The surface coverages (θ_i) are unknown in these equations, however, these can be obtained from the subsequent absorption/desorption processes.

The absorption (J_2^i) and desorption (J_{-2}^i) fluxes [mol s^{-1}] [Eq. (2)] can be written as

$$\begin{cases} J_2^i = \bar{k}_2^i A_i c_i^s(MH) c_i^b(M), \\ J_{-2}^i = \bar{k}_{-2}^i A_i c_i^s(M) c_i^b(MH), \end{cases} \quad i = \alpha, \beta, \tag{20}$$

where $\bar{k}_2^i$ [m^3 mol^{-1} s^{-1}] is the absorption rate constant, $\bar{k}_{-2}^i$ [m^3 mol^{-1} s^{-1}] the desorption rate constant, $c_i^b(M)$ [mol m^{-3}] the bulk concentration of nonoccupied host sites, and $c_i^b(MH)$ [mol m^{-3}] is the bulk concentration of occupied host sites. $c_i^b(M)$ and $c_i^b(MH)$ can be expressed in terms of the number of host sites, guest hydrogen atoms, and phase-normalized hydrogen concentration (x_i) [Eq. (9)] as

$$\begin{cases} c_i^b(M) = \frac{N_i^b - n_i^b}{N_A V_i} = (1 - x_i) \frac{N_i^b}{N_A V_i}, \\ c_i^b(MH) = \frac{n_i^b}{N_A V_i} = x_i \frac{N_i^b}{N_A V_i}, \end{cases} \tag{21}$$

where V_i is the volume of phase i and $N_i^b / N_A V_i$ is a material constant, representing the available host sites per volumetric unit of the bulk. Again normalizing with respect to A_0, this results in the following expressions for the normalized absorption and desorption fluxes [mol m^{-2} s^{-1}]:

$$\begin{cases} j_2^i = k_2^i \theta_i (1 - x_i)(N_i^b / n_{\max}^b), \\ j_{-2}^i = k_{-2}^i x_i (1 - \theta_i)(N_i^b / n_{\max}^b), \end{cases} \tag{22}$$

where $k_2^i = \bar{k}_2^i \left(\frac{N_i^s}{N_A A_i}\right)\left(\frac{N_i^b}{N_A V_i}\right)$ and $k_{-2}^i = \bar{k}_{-2}^i \left(\frac{N_i^s}{N_A A_i}\right)\left(\frac{N_i^b}{N_A V_i}\right)$ are the redefined absorption and desorption rate constants, respectively [mol m^{-2} s^{-1}].

Under equilibrium conditions, the flux of the forward reaction in each phase is again equal to that of the backward reaction ($j_2^i = j_{-2}^i$), which yields a set of equations from which θ_i can be determined, according to

$$k_2^i \theta_i (1 - x_i) = k_{-2}^i x_i (1 - \theta_i). \tag{23}$$

Eliminating θ_i in Eq. (19) by means of Eq. (23) ultimately gives a complex expression for the equilibrium hydrogen pressure as a function x_i and the various rate constants. These rate constants are, however, all temperature dependent, according to the Arrhenius equation

$$k = B \exp\left(\frac{-E^a}{kT}\right), \tag{24}$$

where E^a is the activation energy and B is the pre-exponential or frequency factor of the reaction. In the Arrhenius equation (24), other unknown parameters are introduced, complicating the mathematical evaluation. However, it will be shown in the next section that by adopting the as-denoted rectangular rule this problem can be solved by replacing the activation energies by the atomic hydrogen energies defined in our previously reported LGM.[13]

D. Rectangular rule

The activation energies for the various reaction steps in the present hydrogen storage system are schematically indicated in Fig. 4. The three regions important in the (de)hydrogenation process, can again be recognized in this figure. It is evident that minimum energies can be found for hydrogen in the gas phase, at the surface, and in the bulk of the hydride-forming material. It is generally accepted that the energy of hydrogen is most favorable inside the bulk of hydride-forming compounds.[8]

Considering, for example, the recombination process in more detail, the activation energies of the adsorption and recombination reaction are denoted by E_g^i and E_{θ}^i, respectively. If the energy of a hydrogen molecule in the gas phase is denoted by ε_g and that of an adsorbed hydrogen atom at the surface by ε_{θ}^i, it is obvious from Fig. 4 that

$$\Pi_{g\theta}^i = (E_{\theta}^i + \varepsilon_{\theta}^i) = (E_g^i + \varepsilon_g)/2, \tag{25}$$

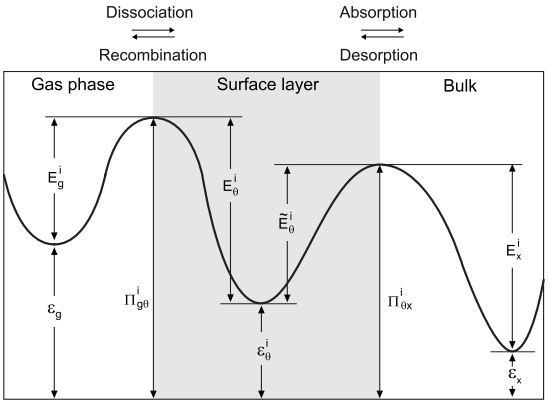

FIG. 4. Energy diagram of the various hydrogen species involved in the (de)hydrogenation system defined in Fig. 2, including the energies of atomic hydrogen in the gas phase (ε_g), at the surface (ε_θ) and in the bulk (ε_x), the various activation energies (E_m^i) and energy barriers (Π_m^i). All energies are given with respect to an arbitrary chosen reference state.

where the energy barrier ($\Pi_{g\theta}^i$) is given with respect to an arbitrary chosen reference state. The expression covered by Eq. (25) will further be denoted as "rectangular rule." Replacing the activation energies in Eq. (24) by means of Eq. (25) yields modified expressions in which the energies of the various hydrogen states (ε_g and ε_θ^i) can be recognized

$$\begin{cases} k_1^i = B_1^i \exp\left(-\dfrac{E_g^i}{kT}\right) \Rightarrow k_1^i = B_1^i \exp\left(-\dfrac{2\Pi_{g\theta}^i}{kT}\right)\exp\left(\dfrac{\varepsilon_g}{kT}\right), \\ k_{-1}^i = B_{-1}^i \exp\left(-\dfrac{2E_\theta^i}{kT}\right) \Rightarrow k_{-1}^i = B_{-1}^i \exp\left(-\dfrac{2\Pi_{g\theta}^i}{kT}\right)\exp\left(\dfrac{2\varepsilon_\theta^i}{kT}\right). \end{cases} \tag{26}$$

Similarly, the energy barrier of the absorption/desorption reaction ($\Pi_{\theta x}^i$) can be described by

$$\Pi_{\theta x}^i = \tilde{E}_\theta^i + \varepsilon_\theta^i = E_x^i + \varepsilon_x, \tag{27}$$

where $\tilde{E}_\theta^i$ is the activation energy of the absorption reaction per hydrogen atom in phase i, E_x^i the activation energy of the desorption reaction, and ε_x is energy of absorbed hydrogen. This leads to

$$\begin{cases} k_2^i = B_2^i \exp\left(-\dfrac{E_\theta^i}{kT}\right) \Rightarrow k_2^i = B_2^i \exp\left(-\dfrac{\Pi_{\theta x}^i}{kT}\right)\exp\left(\dfrac{\varepsilon_\theta^i}{kT}\right), \\ k_{-2}^i = B_{-2}^i \exp\left(-\dfrac{E_x^i}{kT}\right) \Rightarrow k_{-2}^i = B_{-2}^i \exp\left(-\dfrac{\Pi_{\theta x}^i}{kT}\right)\exp\left(\dfrac{\varepsilon_x}{kT}\right). \end{cases} \tag{28}$$

The next section will explain the derivation of expressions for the energies of hydrogen in the three distinct areas of the system, i.e., ε_x, ε_θ and ε_g.

E. Energy description of hydrogen sites

1. Bulk

The general description of the energy of the bulk of a hydride-forming material is based on a mean-field theory and follows from the previously presented LGM.[13] The most relevant characteristics of this LGM are as follows. First, the energy of the various host lattices is considered. The contribution of each unit cell to the total energy has been denoted as L_α and L_β for the α and β phase, respectively.[20,21] Secondly, the so-called Bragg-Williams approximation was adopted, implying that the absorbed hydrogen atoms are randomly distributed in the hydride-forming material.[22] In the case of two-phase coexistence, two energetically different types of host sites coexist in the system and a binary alloy approach has to be adopted. E_α^b and E_β^b represent the energy of individually absorbed hydrogen atoms in both phases. It is, furthermore, assumed that an absorbed hydrogen atom at a particular site can interact with a hydrogen atom at any other site,[23] with a specific interaction energy (U_{ii}^b). According to the mean-field approximation[22] the interaction energy between the occupied sites does not depend on their distance. $U_{\alpha\alpha}^b$ and $U_{\beta\beta}^b$ are the interaction energies between two absorbed atoms in the α and β phase, respectively, and $U_{\alpha\beta}^b$ represents that between two absorbed hydrogen atoms in different phases.[22]

These considerations have led to the following Hamiltonian (U^b) for the bulk of the considered hydrogen storage system

$$U^b = L_\alpha M_\alpha + L_\beta M_\beta + E_\alpha^b n_\alpha^b + E_\beta^b n_\beta^b + \frac{U_{\alpha\alpha}^b}{2n_{\max}^b}(n_\alpha^b)^2 + \frac{U_{\beta\beta}^b}{2n_{\max}^b}(n_\beta^b)^2 + \frac{U_{\alpha\beta}^b}{2n_{\max}^b} n_\alpha^b n_\beta^b. \tag{29}$$

Taking into account the definition of M_α and M_β given in Eq. (3), the first two terms in Eq. (29) can be rewritten as

$$\begin{aligned} L_\alpha M_\alpha + L_\beta M_\beta &= L_\alpha M + (L_\beta - L_\alpha) M_\beta = L_\alpha M + (L_\beta - L_\alpha) N_\beta^b \\ &= L_\alpha M + (L_\beta - L_\alpha) n_{\max}^b (N_\beta^b / n_{\max}^b). \end{aligned} \tag{30}$$

When in addition n_α^b and n_β^b are expressed via x, using Eq. (8), the following relationships are obtained for the three considered crystallographic regions:

$$U^b = n^b_{\max}\begin{cases} \dfrac{L_\alpha M}{n^b_{\max}} + E^b_\alpha\, x + \dfrac{U^b_{\alpha\alpha}}{2}x^2, & x < \mathrm{x}_\alpha, \\ \dfrac{L_\alpha M}{n^b_{\max}} + (L_\beta - L_\alpha)(N^b_\beta/n^b_{\max}) + E^b_\alpha \mathrm{x}_\alpha (N^b_\alpha/n^b_{\max}) + E^b_\beta \mathrm{x}_\beta (N^b_\beta/n^b_{\max}) & \\ \quad + \dfrac{U^b_{\alpha\alpha}\mathrm{x}^2_\alpha}{2}(N^b_\alpha/n^b_{\max})^2 + \dfrac{U^b_{\beta\beta}\mathrm{x}^2_\beta}{2}(N^b_\beta/n^b_{\max})^2 + \dfrac{U^b_{\alpha\beta}\mathrm{x}_\alpha\mathrm{x}_\beta}{2}(N^b_\alpha/n^b_{\max})(N^b_\beta/n^b_{\max}), & \mathrm{x}_\alpha \le x \le \mathrm{x}_\beta, \\ \dfrac{L_\beta M}{n^b_{\max}} + E^b_\beta\, x + \dfrac{U^b_{\beta\beta}}{2}x^2, & x > \mathrm{x}_\beta. \end{cases} \tag{31}$$

ε_x can be obtained by differentiating Eq. (31) with respect to n^b. Since $n^b = x n^b_{\max}$, it follows that $\frac{\partial U^b}{\partial n^b}\Delta n^b = \frac{\partial U^b}{\partial n^b}\cdot 1 = \frac{1}{n^b_{\max}}\frac{\partial U^b}{\partial x}$, which ultimately leads to

$$\varepsilon_x = \frac{1}{n^b_{\max}}\frac{\partial U^b}{\partial x} = \begin{cases} E^b_\alpha + U^b_{\alpha\alpha}x, & x < \mathrm{x}_\alpha \\ \dfrac{E^b_\beta \mathrm{x}_\beta - E^b_\alpha \mathrm{x}_\alpha - U^b_{\alpha\alpha}\mathrm{x}^2_\alpha (N^b_\alpha/n^b_{\max}) + U^b_{\alpha\beta}\mathrm{x}^2_\beta (N^b_\beta/n^b_{\max}) + U^b_{\beta\beta}\mathrm{x}_\alpha\mathrm{x}_\beta (N^b_\alpha/n^b_{\max} - N^b_\beta/n^b_{\max})/2 + L}{\mathrm{x}_\beta - \mathrm{x}_\alpha}, & \mathrm{x}_\alpha \le x \le \mathrm{x}_\beta, \\ E^b_\beta + U^b_{\beta\beta}x, & x > \mathrm{x}_\beta \end{cases} \tag{32}$$

in which $L = L_\beta - L_\alpha$.[13] Since n^b_α and n^b_β are interdependent variables in the two-phase coexistence region [see Eq. (8)] ε^α_x and ε^β_x are equal in this region and can therefore be replaced by ε_x in Eq. (32).

2. Surface

Adopting a similar mean-field approach for the energy of adsorbed hydrogen at the surface as for the bulk, the following surface Hamiltonian (U^s) is obtained:

$$U^s = E^s_\alpha n^s_\alpha + E^s_\beta n^s_\beta + \frac{U^s_{\alpha\alpha}(n^s_\alpha)^2}{2n^s_{\max}} + \frac{U^s_{\beta\beta}(n^s_\beta)^2}{2n^s_{\max}} + \frac{U^s_{\alpha\beta}n^s_\alpha n^s_\beta}{2n^s_{\max}}, \tag{33}$$

where E^s_i represent the energies of an individually adsorbed hydrogen atom at the surface, U^s_{ii} are the interaction energies between these atoms in the various phases, and n^s_i is the number of adsorbed atoms.

The surface Hamiltonian (33) is different from that for the bulk [Eq. (29)] in two aspects: (i) the first two terms, associated with the crystal lattice are absent since no host lattice is involved in this region and (ii) n^s_α and n^s_β are independent variables as these variables are determined by the bulk concentrations. Expressions for ε^i_θ are obtained by differentiating Eq. (33) with respect to n^s_α and n^s_β, leading to

$$\begin{aligned} \varepsilon^\alpha_\theta &= \frac{\partial U^s}{\partial n^s_\alpha} = E^s_\alpha + U^s_{\alpha\alpha}\frac{n^s_\alpha}{n^s_{\max}} + U^s_{\alpha\beta}\frac{n^s_\beta}{n^s_{\max}} = E^s_\alpha + U^s_{\alpha\alpha}\theta^\alpha \\ &\quad + U^s_{\alpha\beta}\theta^\beta/2, \\ \varepsilon^\beta_\theta &= \frac{\partial U^s}{\partial n^s_\beta} = E^s_\beta + U^s_{\beta\beta}\frac{n^s_\beta}{n^s_{\max}} + U^s_{\alpha\beta}\frac{n^s_\alpha}{n^s_{\max}} = E^s_\beta + U^s_{\beta\beta}\theta^\beta \\ &\quad + U^s_{\alpha\beta}\theta^\alpha/2. \end{aligned} \tag{34}$$

3. Gas phase

To describe the energy of hydrogen in the gas phase we applied a similar mean-field concept as for the absorbed and adsorbed state. This leads to the following simple Hamiltonian (U^g):

$$U^g = E^g n^g, \tag{35}$$

where E^g represents the energy of an individual hydrogen molecule and n^g is the number of hydrogen molecules present in the gas phase. Differentiating Eq. (35) with respect to n^g leads to $\varepsilon_g = \frac{\partial U^g}{\partial n^g} = E^g$. The internal energy of two-atomic ideal gasses is generally described[24] by $E^g = 5kT/2$, which leads to the following expression:

$$\varepsilon_g = \frac{5}{2}kT. \tag{36}$$

F. Final equations

Substituting ε_x [Eq. (32)] and ε_θ [Eq. (34)] into Eq. (28), the following expressions for the absorption and desorption rate constants are obtained:

$$k_2^{\alpha} = B_2^{\alpha} \exp\left(-\frac{\Pi_{\theta x}^{\alpha}}{kT}\right)\exp\left(\frac{E_{\alpha}^{s} + U_{\alpha\alpha}^{s}\theta^{\alpha} + U_{\alpha\beta}^{s}\theta^{\beta}/2}{(kT/e)}\right), \quad k_2^{\beta} = B_2^{\beta} \exp\left(-\frac{\Pi_{\theta x}^{\beta}}{kT}\right)\exp\left(\frac{E_{\beta}^{s} + U_{\beta\beta}^{s}\theta^{\beta} + U_{\alpha\beta}^{s}\theta^{\alpha}/2}{(kT/e)}\right),$$

$$k_{-2}^{\alpha} = B_{-2}^{\alpha} \exp\left(-\frac{\Pi_{\theta x}^{\alpha}}{kT}\right)\begin{cases} \exp\left(\dfrac{E_{\alpha}^{b} + U_{\alpha\alpha}^{b}x}{(kT/e)}\right), & x < \mathrm{x}_{\alpha}, \\ \exp\left(\dfrac{E_{\beta}^{b}\mathrm{x}_{\beta} - E_{\alpha}^{b}\mathrm{x}_{\alpha} - U_{\alpha\alpha}^{b}\mathrm{x}_{\alpha}^{2}\dfrac{N_{\alpha}^{b}}{n_{\max}^{b}} + U_{\beta\beta}^{b}\mathrm{x}_{\beta}^{2}\dfrac{N_{\beta}^{b}}{n_{\max}^{b}} + U_{\alpha\beta}^{b}\mathrm{x}_{\alpha}\mathrm{x}_{\beta}\left(\dfrac{N_{\alpha}^{b}}{n_{\max}^{b}} - \dfrac{N_{\beta}^{b}}{n_{\max}^{b}}\right)/2 + L}{(kT/e)(\mathrm{x}_{\beta} - \mathrm{x}_{\alpha})}\right), & \mathrm{x}_{\alpha} \le x \le \mathrm{x}_{\beta}, \end{cases} \tag{37}$$

$$k_{-2}^{\beta} = B_{-2}^{\beta} \exp\left(-\frac{\Pi_{\theta x}^{\beta}}{kT}\right)\begin{cases} \exp\left(\dfrac{E_{\beta}^{b}\mathrm{x}_{\beta} - E_{\alpha}^{b}\mathrm{x}_{\alpha} - U_{\alpha\alpha}^{b}\mathrm{x}_{\alpha}^{2}\dfrac{N_{\alpha}^{b}}{n_{\max}^{b}} + U_{\beta\beta}^{b}\mathrm{x}_{\beta}^{2}\dfrac{N_{\beta}^{b}}{n_{\max}^{b}} + U_{\alpha\beta}^{b}\mathrm{x}_{\alpha}\mathrm{x}_{\beta}\left(\dfrac{N_{\alpha}^{b}}{n_{\max}^{b}} - \dfrac{N_{\beta}^{b}}{n_{\max}^{b}}\right)/2 + L}{(kT/e)(\mathrm{x}_{\beta} - \mathrm{x}_{\alpha})}\right), & \mathrm{x}_{\alpha} \le x \le \mathrm{x}_{\beta}, \\ \exp\left(\dfrac{E_{\beta}^{b} + U_{\beta\beta}^{b}x}{(kT/e)}\right), & x > \mathrm{x}_{\beta}. \end{cases} \tag{37}$$

Eliminating these rate constants in Eq. (23), the following set of equations are obtained for the surface coverages in the three considered crystallographic regions

$$\begin{cases} \dfrac{x(1-\theta)}{\theta(1-x)} = \dfrac{B_2^{\alpha}}{B_{-2}^{\alpha}}\exp\left(\dfrac{E_{\alpha}^{s} + U_{\alpha\alpha}^{s}\theta - (E_{\alpha}^{b} + U_{\alpha\alpha}^{b}x)}{(RT/F)}\right), & 0 \le x < \mathrm{x}_{\alpha}, \\ \dfrac{x_i(1-\theta_i)}{\theta_i(1-x_i)} = \dfrac{B_2^{i}}{B_{-2}^{i}}\exp\left(\dfrac{E_{i}^{s} + U_{ii}^{s}\theta^{i} + U_{\alpha\beta}^{s}\theta^{j}/2}{(RT/F)} - \dfrac{E_{\beta}^{b}\mathrm{x}_{\beta} - E_{\alpha}^{b}\mathrm{x}_{\alpha} - U_{\alpha\alpha}^{b}\mathrm{x}_{\alpha}^{2}\dfrac{N_{\alpha}^{b}}{n_{\max}^{b}} + U_{\beta\beta}^{b}\mathrm{x}_{\beta}^{2}\dfrac{N_{\beta}^{b}}{n_{\max}^{b}} + U_{\alpha\beta}^{b}\mathrm{x}_{\alpha}\mathrm{x}_{\beta}\left(\dfrac{N_{\alpha}^{b}}{n_{\max}^{b}} - \dfrac{N_{\beta}^{b}}{n_{\max}^{b}}\right)/2 + L}{(RT/F)(\mathrm{x}_{\beta} - \mathrm{x}_{\alpha})}\right), & \mathrm{x}_{\alpha} \le x \le \mathrm{x}_{\beta}, \\ \dfrac{x(1-\theta)}{\theta(1-x)} = \dfrac{B_2^{\beta}}{B_{-2}^{\beta}}\exp\left(\dfrac{E_{\beta}^{s} + U_{\beta\beta}^{s}\theta - (E_{\beta}^{b} + U_{\beta\beta}^{b}x)}{(RT/F)}\right), & \mathrm{x}_{\beta} < x \le 1, \end{cases} \tag{38}$$

where $j = \alpha$ when $i = \beta$ and *visa versa*. Elegantly, it should be noted that the introduced energy barriers $\Pi_{\theta x}^{\alpha}$ and $\Pi_{\theta x}^{\beta}$ are both eliminated under the considered equilibrium conditions.

Substituting ε_x [Eq. (34)] and ε_θ [Eq. (36)] in Eq. (26) and eliminating the obtained rate constants in the pressure relationship represented by Eq. (19) yield general expressions for the pressure-composition isotherms, according to

$$P_{\mathrm{H}_2}^{\mathrm{eq}} = RT$$

$$\times\begin{cases} \left(\dfrac{\theta}{1-\theta}\right)^2 \dfrac{B_{-1}^{\alpha}}{B_1^{\alpha}}\exp\left(2\dfrac{E_{\alpha}^{s} + U_{\alpha\alpha}^{s}\theta}{(RT/F)}\right)\exp(-5/2), & 0 \le x < \mathrm{x}_{\alpha}, \\ \dfrac{\left[B_{-1}^{\alpha}\exp\left(2\dfrac{E_{\alpha}^{s} + U_{\alpha\alpha}^{s}\theta^{\alpha} + U_{\alpha\beta}^{s}\theta^{\beta}/2}{(RT/F)}\right)(\theta_{\alpha})^2(N_{\alpha}^{b}/n_{\max}^{b}) + B_{-1}^{\beta}\exp\left(\dfrac{\Delta\Pi}{kT}\right)\exp\left(2\dfrac{E_{\beta}^{s} + U_{\beta\beta}^{s}\theta^{\beta} + U_{\alpha\beta}^{s}\theta^{\alpha}/2}{(RT/F)}\right)(\theta_{\beta})^2(N_{\beta}^{b}/n_{\max}^{b})\right]}{\left[B_1^{\alpha}(1-\theta_{\alpha})^2(N_{\alpha}^{b}/n_{\max}^{b}) + B_1^{\beta}\exp\left(\dfrac{\Delta\Pi}{kT}\right)(1-\theta_{\beta})^2(N_{\beta}^{b}/n_{\max}^{b})\right]\exp(5/2)}, & \mathrm{x}_{\alpha} \le x \le \mathrm{x}_{\beta}, \\ \left(\dfrac{\theta}{1-\theta}\right)^2 \dfrac{B_{-1}^{\beta}}{B_1^{\beta}}\exp\left(2\dfrac{E_{\beta}^{s} + U_{\beta\beta}^{s}\theta}{(RT/F)}\right)\exp(-5/2), & \mathrm{x}_{\beta} < x \le 1, \end{cases} \tag{39}$$

where $\Delta\Pi=2(\Pi^{\alpha}_{g\theta}-\Pi^{\beta}_{g\theta})$. Equations (38) and (39) describe the fundamental relationships between the equilibrium hydrogen partial pressure, surface coverages, hydrogen concentrations, and parameters of the hydrogen storage system. Obviously, the various parameter values obtained from the LGM (Ref. 13) are very useful in this respect.

G. Model simplifications

The set of equations given in Eq. (38) is a complex highly nonlinear two-dimensional system with two unknowns. An analytical solution is not possible and the various surface coverages can therefore only be numerically obtained. In order to reduce the complexity of the system some basic physical assumptions (A) are applied to Eqs. (38) and (39).

(A1) Surface interphase interactions can be considered negligible ($U^{s}_{\alpha\beta}=0$) as the interaction energies between adsorbed hydrogen atoms at the surface are expected to be much lower than those in the absorbed state. In addition, the presence of α-β transition regions will be very limited in a two-dimensional surface structure and will therefore hardly contribute to the entire surface energy.

(A2) The energy barriers for the hydrogen dissociation reaction are considered to be phase independent, i.e., $\Delta\Pi=2(\Pi^{\alpha}_{g\theta}-\Pi^{\beta}_{g\theta})=0$.

The set of equations (38) and (39) depends on the large number of parameters, which are physically meaningful but not always identifiable from the analysis of pressure-composition isotherms. Some identification restrictions (I) have to be set for a proper estimation of the system.

(I1) Since only the ratios of the individual corresponding B values can be identified, the following parameters are introduced:

$$\mathrm{B}^{\alpha}_{1}=B^{\alpha}_{-1}/B^{\alpha}_{1},\quad \mathrm{B}^{\beta}_{1}=B^{\beta}_{-1}/B^{\beta}_{1},$$

$$\mathrm{B}^{\alpha\beta}_{1}=B^{\alpha}_{1}/B^{\beta}_{1},\quad \mathrm{B}^{\alpha}_{2}=B^{\alpha}_{2}/B^{\alpha}_{-2},\quad \mathrm{B}^{\beta}_{2}=B^{\beta}_{2}/B^{\beta}_{-2}. \tag{40}$$

(I2) Since the new parameters B^{β}_{1} and $\mathrm{B}^{\alpha\beta}_{1}$ are only used in combination $\mathrm{B}^{\beta}_{1}/\mathrm{B}^{\alpha\beta}_{1}$ [Eq. (39) for the two-phase coexistence region], $\mathrm{B}^{\alpha\beta}_{1}$ is normalized to unity

$$\mathrm{B}^{\alpha\beta}_{1}=1. \tag{41}$$

Taking into account the above assumptions, this results in the following set of equations for the surface coverages.

$$\begin{cases} \dfrac{x(1-\theta)}{\theta(1-x)}=\mathrm{B}^{\alpha}_{2}\exp\left(\dfrac{E^{s}_{\alpha}+U^{s}_{\alpha\alpha}\theta-(E^{b}_{\alpha}+U^{b}_{\alpha\alpha}x)}{(RT/F)}\right), & 0\le x<\mathrm{x}_{\alpha}, \\ \dfrac{x_{\alpha}(1-\theta_{\alpha})}{\theta_{\alpha}(1-x_{\alpha})}=\mathrm{B}^{\alpha}_{2}\exp\left(\dfrac{E^{s}_{\alpha}+U^{s}_{\alpha\alpha}\theta^{\alpha}}{(RT/F)}-\dfrac{E^{b}_{\beta}\mathrm{x}_{\beta}-E^{b}_{\alpha}\mathrm{x}_{\alpha}-U^{b}_{\alpha\alpha}\mathrm{x}^{2}_{\alpha}\dfrac{N^{b}_{\alpha}}{n^{b}_{\max}}+U^{b}_{\beta\beta}\mathrm{x}^{2}_{\beta}\dfrac{N^{b}_{\beta}}{n^{b}_{\max}}+U^{b}_{\alpha\beta}\mathrm{x}_{\alpha}\mathrm{x}_{\beta}\left(\dfrac{N^{b}_{\alpha}}{n^{b}_{\max}}-\dfrac{N^{b}_{\beta}}{n^{b}_{\max}}\right)/2+L}{(RT/F)(\mathrm{x}_{\beta}-\mathrm{x}_{\alpha})}\right), & \mathrm{x}_{\alpha}\le x\le\mathrm{x}_{\beta} \end{cases} \tag{42a}$$

and

$$\begin{cases} \dfrac{x_{\beta}(1-\theta_{\beta})}{\theta_{\beta}(1-x_{\beta})}=\mathrm{B}^{\beta}_{2}\exp\left(\dfrac{E^{s}_{\beta}+U^{s}_{\beta\beta}\theta^{\beta}}{(RT/F)}-\dfrac{E^{b}_{\beta}\mathrm{x}_{\beta}-E^{b}_{\alpha}\mathrm{x}_{\alpha}-U^{b}_{\alpha\alpha}\mathrm{x}^{2}_{\alpha}\dfrac{N^{b}_{\alpha}}{n^{b}_{\max}}+U^{b}_{\beta\beta}\mathrm{x}^{2}_{\beta}\dfrac{N^{b}_{\beta}}{n^{b}_{\max}}+U^{b}_{\alpha\beta}\mathrm{x}_{\alpha}\mathrm{x}_{\beta}\left(\dfrac{N^{b}_{\alpha}}{n^{b}_{\max}}-\dfrac{N^{b}_{\beta}}{n^{b}_{\max}}\right)/2+L}{(RT/F)(\mathrm{x}_{\beta}-\mathrm{x}_{\alpha})}\right), & \mathrm{x}_{\alpha}\le x\le\mathrm{x}_{\beta}, \\ \dfrac{x(1-\theta)}{\theta(1-x)}=\mathrm{B}^{\beta}_{2}\exp\left(\dfrac{E^{s}_{\beta}+U^{s}_{\beta\beta}\theta-(E^{b}_{\beta}+U^{b}_{\beta\beta}x)}{(RT/F)}\right), & \mathrm{x}_{\beta}<x\le 1. \end{cases} \tag{42b}$$

The equilibrium pressure can then be represented by

$$P^{\mathrm{eq}}_{\mathrm{H}_2}=RT\begin{cases} \left(\dfrac{\theta}{1-\theta}\right)^{2}\mathrm{B}^{\alpha}_{1}\exp\left(2\dfrac{E^{s}_{\alpha}+U^{s}_{\alpha\alpha}\theta}{(RT/F)}\right)\exp(-5/2), & 0\le x<\mathrm{x}_{\alpha}, \\ \dfrac{\left[\mathrm{B}^{\alpha}_{1}\exp\left(2\dfrac{E^{s}_{\alpha}+U^{s}_{\alpha\alpha}\theta^{\alpha}}{(RT/F)}\right)(\theta_{\alpha})^{2}N^{b}_{\alpha}/n^{b}_{\max}+\mathrm{B}^{\beta}_{1}\exp\left(2\dfrac{E^{s}_{\beta}+U^{s}_{\beta\beta}\theta^{\beta}}{(RT/F)}\right)(\theta_{\beta})^{2}N^{b}_{\beta}/n^{b}_{\max}\right]}{[(1-\theta_{\alpha})^{2}N^{b}_{\alpha}/n^{b}_{\max}+(1-\theta_{\beta})^{2}N^{b}_{\beta}/n^{b}_{\max}]\exp(5/2)}, & \mathrm{x}_{\alpha}\le x\le\mathrm{x}_{\beta}, \\ \left(\dfrac{\theta}{1-\theta}\right)^{2}\mathrm{B}^{\beta}_{1}\exp\left(2\dfrac{E^{s}_{\beta}+U^{s}_{\beta\beta}\theta}{(RT/F)}\right)\exp(-5/2), & \mathrm{x}_{\beta}<x\le 1 \end{cases} \tag{43}$$

and all considered reactions fluxes by

$$j_1 = \exp\left(\frac{5}{2}\right)\frac{P_{H_2}^{eq}}{RT}\begin{cases}(1-\theta)^2, & 0 \le x < x_\alpha,\\ (1-\theta_\alpha)^2 N_\alpha^b/n_{max}^b + (1-\theta_\beta)^2 N_\beta^b/n_{max}^b, & x_\alpha \le x \le x_\beta,\\ (1-\theta)^2, & x_\beta < x \le 1,\end{cases} \tag{44a}$$

$$j_{-1} = \begin{cases} B_1^\alpha \theta^2 \exp\left(2\dfrac{E_\alpha^s + U_{\alpha\alpha}^s \theta}{(RT/F)}\right), & 0 \le x < x_\alpha,\\ B_1^\alpha \exp\left(2\dfrac{E_\alpha^s + U_{\alpha\alpha}^s \theta^\alpha}{(RT/F)}\right)(\theta_\alpha)^2 N_\alpha^b/n_{max}^b + B_1^\beta \exp\left(2\dfrac{E_\beta^s + U_{\beta\beta}^s \theta^\beta}{(RT/F)}\right)(\theta_\beta)^2 N_\beta^b/n_{max}^b, & x_\alpha \le x \le x_\beta,\\ B_1^\beta \theta^2 \exp\left(2\dfrac{E_\beta^s + U_{\beta\beta}^s \theta}{(RT/F)}\right), & x_\beta < x \le 1,\end{cases} \tag{44b}$$

$$j_2 = \begin{cases} B_2^\alpha \exp\left(\dfrac{E_\alpha^s + U_{\alpha\alpha}^s \theta}{(RT/F)}\right)\theta(1-x), & 0 \le x < x_\alpha,\\ B_2^\alpha \exp\left(2\dfrac{E_\alpha^s + U_{\alpha\alpha}^s \theta^\alpha}{(RT/F)}\right)\theta_\alpha(1-x_\alpha) N_\alpha^b/n_{max}^b + B_2^\beta \exp\left(2\dfrac{E_\beta^s + U_{\beta\beta}^s \theta^\beta}{(RT/F)}\right)\theta_\beta(1-x_\beta) N_\beta^b/n_{max}^b, & x_\alpha \le x \le x_\beta,\\ B_2^\beta \exp\left(2\dfrac{E_\beta^s + U_{\beta\beta}^s \theta}{(RT/F)}\right)\theta(1-x), & x_\beta < x \le 1,\end{cases} \tag{44c}$$

$$j_{-2} = \begin{cases} \exp\left(\dfrac{E_\alpha^b + U_{\alpha\alpha}^b x}{(RT/F)}\right)x(1-\theta), & 0 \le x < x_\alpha,\\ \exp\left(\dfrac{E_\beta^b x_\beta - E_\alpha^b x_\alpha - U_{\alpha\alpha}^b x_\alpha^2 N_\alpha^b/n_{max}^b + U_{\beta\beta}^b x_\beta^2 N_\beta^b/n_{max}^b + U_{\alpha\beta}^b x_\alpha x_\beta (N_\alpha^b/n_{max}^b - N_\beta^b/n_{max}^b)/2 + L}{(RT/F)(x_\beta - x_\alpha)}\right) & \\ \qquad \times [(1-\theta_\alpha)x_\alpha N_\alpha^b/n_{max}^b + (1-\theta_\beta)x_\beta N_\beta^b/n_{max}^b], & x_\alpha \le x \le x_\beta,\\ \exp\left(\dfrac{E_\beta^b + U_{\beta\beta}^b x}{(RT/F)}\right)x(1-\theta), & x_\beta < x \le 1.\end{cases} \tag{44d}$$

Expressions for the fluxes are the final equations. Some additional refinements can, however, be made for the equilibrium pressure and surface coverage equations.

(I3) To avoid a problem of identification two new parameters are introduced, according to

$$P_i = RT\frac{B_1^i}{(B_2^i)^2}\exp(-5/2). \tag{45}$$

(I4) Finally, the following normalization is applied:

$$E_\alpha^s = 0 \quad \text{and} \quad E_\beta^s = 0. \tag{46}$$

The reason for normalization [Eq. (46)] is that E_α^s and E_β^s enters Eqs. (42a) and (42b) always as products $B_2^\alpha e^{E_\alpha^s/(RT/F)}$ and $B_2^\beta e^{E_\beta^s/(RT/F)}$, respectively, and can therefore not be separately identified from B_2^α and B_2^β.

The above limitations results in the following expressions for the equilibrium pressure:

$$P_{\mathrm{H}_2}^{\mathrm{eq}} = \begin{cases} P_\alpha \left(\dfrac{x}{1-x}\right)^2 \exp\left(2\dfrac{E_\alpha^b + U_{\alpha\alpha}^b x}{(RT/F)}\right), & 0 \le x \le \mathrm{x}_\alpha, \\ \dfrac{P_\alpha \dfrac{x_\alpha^2(1-\theta_\alpha)^2}{(1-x_\alpha)^2}\dfrac{N_\alpha^b}{n_{\max}^b} + P_\beta \dfrac{x_\beta^2(1-\theta_\beta)^2}{(1-x_\beta)^2}\dfrac{N_\beta^b}{n_{\max}^b}}{(1-\theta_\alpha)^2\dfrac{N_\alpha^b}{n_{\max}^b} + (1-\theta_\beta)^2\dfrac{N_\beta^b}{n_{\max}^b}} \exp[2H_x(x)], & \mathrm{x}_\alpha \le x \le \mathrm{x}_\beta, \\ P_\beta \left(\dfrac{x}{1-x}\right)^2 \exp\left(2\dfrac{E_\beta^b + U_{\beta\beta}^b x}{(RT/F)}\right), & \mathrm{x}_\beta \le x < 1, \end{cases} \tag{47}$$

where

$$H_x(x) = \frac{F}{RT(\mathrm{x}_\beta - \mathrm{x}_\alpha)}\left(E_\beta^b \mathrm{x}_\beta - E_\alpha^b \mathrm{x}_\alpha - U_{\alpha\alpha}^b \mathrm{x}_\alpha^2 \frac{N_\alpha^b}{n_{\max}^b} + U_{\beta\beta}^b \mathrm{x}_\beta^2 \frac{N_\beta^b}{n_{\max}^b} + U_{\alpha\beta}^b \mathrm{x}_\alpha \mathrm{x}_\beta \left(\frac{N_\alpha^b}{n_{\max}^b} - \frac{N_\beta^b}{n_{\max}^b}\right)/2 + L\right). \tag{48}$$

The continuity of the surface coverage θ in point x_α, as defined by Eq. (42a), requires that

$$(E_\beta^b \mathrm{x}_\beta - E_\alpha^b \mathrm{x}_\alpha - U_{\alpha\alpha}^b \mathrm{x}_\alpha^2 + U_{\alpha\beta}^b \mathrm{x}_\alpha \mathrm{x}_\beta/2 + L)/(\mathrm{x}_\beta - \mathrm{x}_\alpha) = E_\alpha^b + U_{\alpha\alpha}^b \mathrm{x}_\alpha. \tag{49}$$

Similarly, by considering Eq. (42b), the continuity condition in phase transition point x_β is obtained

$$(E_\beta^b \mathrm{x}_\beta - E_\alpha^b \mathrm{x}_\alpha + U_{\beta\beta}^b \mathrm{x}_\beta^2 - U_{\alpha\beta}^b \mathrm{x}_\alpha \mathrm{x}_\beta/2 + L)/(\mathrm{x}_\beta - \mathrm{x}_\alpha) = E_\beta^b + U_{\beta\beta}^b \mathrm{x}_\beta. \tag{50}$$

Equations (49) and (50) can be solved for any two parameters, thus providing additional restrictions on the set of model parameters.

III. RESULTS AND DISCUSSION

The presented equilibrium kinetic model has been tested using the experimental data reported for various AB_5-type hydrogen storage materials. These materials have been thoroughly characterized with respect to their physical and (electro)chemical performance. The isotherms for both model-type materials and commercial, misch-metal-based, hydride-forming materials have been simulated as a function of composition and temperature.

The experimental absorption isotherms were measured with a conventional "Sieverts-type" apparatus by expanding a known amount of gas or vacuum into an *in situ* XRD cell and allowing the system to come to equilibrium after each pressure change.[3,25,26] The *in situ* XRD measurements allowed obtaining crystallographic information of the system as a function of hydrogen content. Since all considered materials appear to have the same, hexagonal, crystallographic structure for both the α and β phase, it is evident that the number of host sites per unit cell remains constant and hence that d^b in Eq. (4) is considered unity in the present simulations.

Figure 5(a) shows the agreement between the experimentally measured (symbols) and simulated (line) pressure-composition isotherm for the stoichiometric $LaNi_{4.0}Cu_{1.0}$. The simulation has been carried out according to Eqs. (42) and (47). The numerical values of the model parameters were obtained by nonlinear least-square method and are listed in Table I. The conditions under which the simulations have been carried out will be discussed below.

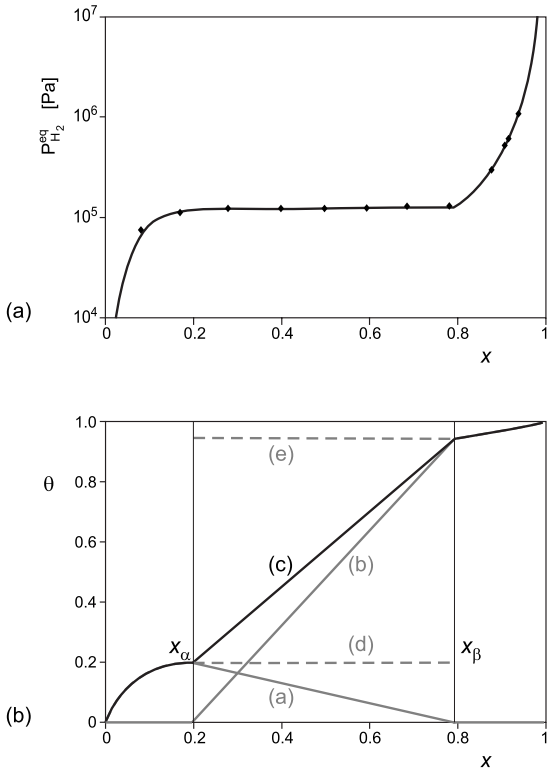

FIG. 5. (a) Measured (Refs. 3, 25, and 26) (symbols) and calculated (line) pressure-composition isotherm for stoichiometric $LaNi_{4.0}Cu_{1.0}$ at 20 °C. (b) Partial surface coverage (θ^i) at the α phase [curve (a)] and β phase [curve (b)] and phase-normalized (θ_i) surface coverages [curves (c) and (d), respectively] as a function of hydrogen content and total surface coverage [curve (e)].

TABLE I. Simulated parameter values under equilibrium kinetic conditions for various non-stoichiometric AB_{5+x} materials at room temperature. Bold parameters are obtained by optimization.

N	Par	Dimension	$LaNi_{4.0}Cu_{1.0}$	$LaNi_{4.2}Cu_{1.0}$	$LaNi_{4.4}Cu_{1.0}$	$LaNi_{5.0}Cu_{1.0}$
1	x_α	[a]	0.196	0.231	0.276	0.346
2	x_β	[a]	0.794	0.711	0.448	0.346
3	E^b_α	eV[a]	0.069	0.070	0.072	0.046
4	E^b_β	eV	**0.079**	**0.067**	**0.074**	0.069[a]
5	$U^b_{\alpha\alpha}$	eV[a]	−0.158	−0.139	−0.122	−0.026
6	$U^b_{\beta\beta}$	eV[a]	−0.053	−0.042	−0.080	−0.092
7	$U^b_{\alpha\beta}$	eV[b]	−0.250	−0.173	−0.205	
8	L	eV[b]	−0.013	−0.007	−0.003	
9	B^α_1	[b]	10.17×10^3	1.31×10^3	0.17×10^3	
10	B^β_1	[b]	2.4	9.0	116.3	
11	B^α_2		**4.509**	**1.615**	**0.580**	
12	B^β_2	[c]	1	1	1	
13	P_α	Pa[c]	10^5	10^5	10^5	10^5
14	P_β	Pa	$\mathbf{0.47\times10^3}$	$\mathbf{1.81\times10^3}$	$\mathbf{23.25\times10^3}$	
15	E^s_α	eV[c]	0	0	0	
16	E^s_β	eV[c]	0	0	0	
17	$U^s_{\alpha\alpha}$	eV[c]	0	0	0	
18	$U^s_{\beta\beta}$	eV[c]	0	0	0	

[a]Parameters are taken from the lattice gas model (Ref. 13).
[b]Parameters are calculated from the continuity conditions.
[c]Parameters are set constant by normalization.

The LGM parameters reported before[13] are used in the present kinetic model (e.g., phase transition points x_α and x_β). P_i in Eq. (47) cannot be separately identified since multiplication of both parameters by the same number may be exactly compensated by some additive term in Eq. (48), e.g., by E^b_α. To avoid identification problems and emphasize the relationship with the LGM, P_α was set to normal atmospheric pressure (10^5 Pa) in the simulations. After preliminary calculations the influence of $U^s_{\alpha\alpha}$ and $U^s_{\beta\beta}$ was found to be extremely small. These parameters were therefore set to zero. Parameters B^α_2, E^b_β and P_β were then determined in the simulation (see Table I), while the remaining parameters $U^b_{\alpha\beta}$ and L were obtained from the continuity conditions Eqs. (49) and (50). Conclusively, the whole pressure composition isotherm can be described by just these three parameters.

Figure 5(a) reveals that the kinetic model describes the hydrogen absorption isotherm of the stoichiometric $LaNi_{4.0}Cu_{1.0}$ material quite well. Three regions can be clearly distinguished: a solid-solution region at low hydrogen concentration ($x<0.196$), a long almost flat two-phase coexistence plateau region ($0.196\leq x\leq 0.794$) and a solid-solution region at high hydrogen concentration ($x>0.794$).

The beauty of the present model is that it makes the complex hydrogen storage system much more transparent. Figure 5(b) illustrates the development of the various calculated surface coverages as a function of hydrogen concentration. In the α solid-solution region θ^α increases sharply at low hydrogen concentration and levels off near the maximum value at phase-transition point x_α [curve (a)]. In the two-phase coexistence region θ^α decreases linearly to become zero in the β solid-solution region. Obviously, the partial surface coverage of the β phase, θ^β [curve (b)] develops in the opposite way. The summation of both partial surface coverages yields the total surface coverage $\theta=\theta^\alpha+\theta^\beta$, which is represented by curve (c). According to Eq. (12) phase-normalized surface coverages for the α and β phase (θ_α and θ_β) were calculated and represented by curves (d) and (e) in Fig. 5(b). The phase-normalized surface coverages remain constant in the two-phase coexisting region and coincide with partial surface coverages in both solid-solution regions.

A distinctive feature of the kinetic model is its ability to reveal detailed information about the various kinetic steps of the hydrogen (de)sorption process. Figure 6 represents, for example, the normalized fluxes under equilibrium conditions for the two basic reactions taking place during hydrogen storage [Eqs. (1) and (2)]. The dissociation and recombination fluxes are shown in curves (a) and (b) of Fig. 6(a), respectively. The hydrogen flux from the gas phase to the surface of the hydride-forming material corresponding to the dissociation reaction is defined here as positive. As expected under equilibrium conditions, the dissociation and recombination fluxes are exactly counterbalancing each other. These fluxes are small in the very early stages of the α-phase solid-solution region. When the hydrogen concentration inside the hydride-forming material grows, the fluxes increase and the maximums are reached at the phase transition point x_α. In the two-phase coexistence region both fluxes go down significantly until the minima are reached at x_β. On the other hand, in the β solid-solution region the fluxes become more or less concentration independent. It can be concluded that for $LaNi_{4.0}Cu_{1.0}$ stoichiometric hydrogen storage material the

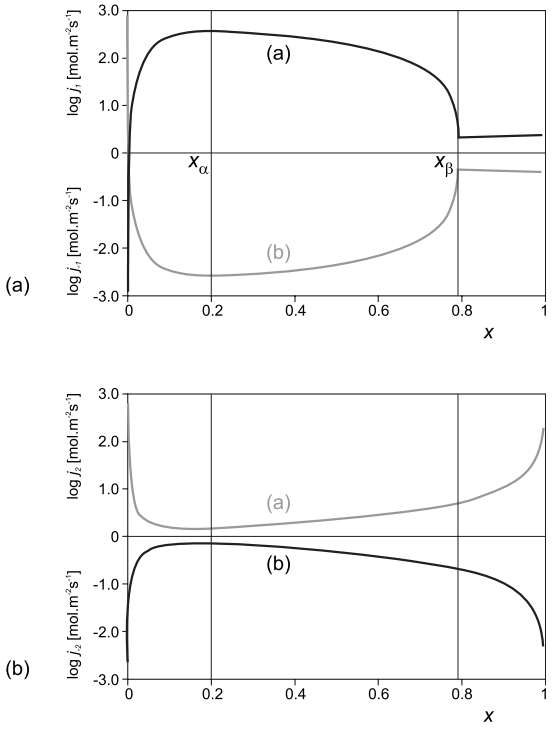

FIG. 6. (a) Normalized dissociation [curve (a)] and recombination [curve (b)] fluxes as a function of normalized hydrogen content (x) under equilibrium conditions for $LaNi_{4.0}Cu_{1.0}$ at 20 °C. (b) Normalized absorption [curve (a)] and desorption [curve (b)] fluxes.

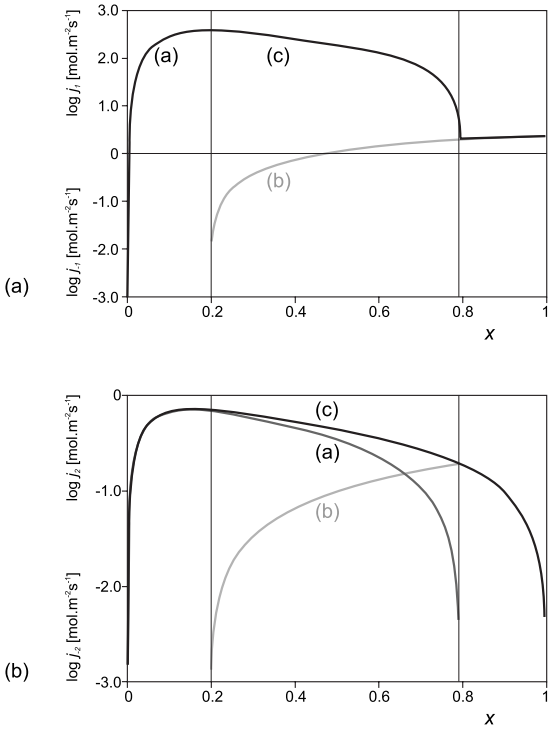

FIG. 7. (a) Partial dissociation fluxes at the α [curve (a)] and β phase [curve (b)] and total dissociation flux [curve (c)] as a function of normalized hydrogen content (x) under equilibrium conditions for $LaNi_{4.0}Cu_{1.0}$. (b) Partial [curves (a) and (b), respectively] and total absorption fluxes [curve (c)].

gas-surface kinetics in the α phase is substantially faster than in the β phase. The same conclusion also holds for the absorption [curve (a) in Fig. 6(b)] and desorption reaction [curve (b)].

All reaction fluxes for $LaNi_{4.0}Cu_{1.0}$ can be further analyzed. Figure 7(a) gives more detailed information on how the normalized dissociation fluxes are built up from the partial fluxes of the individual phases. Obviously, in the pure α phase the α flux [curve (a)] coincides with the total flux [curve (c)]. As soon as phase transition occurs, the surface of the α phase gradually decreases in favor of the β phase. Consequently, the contribution of the α phase to the total flux reduces. At the end of the two-phase coexistence region the total flux is composed of the flux via the β phase surface only. For this particular material, the α-phase flux contribution dominates over that of the β phase [curves (a) and (c) in Fig. 7(a)]. The partial flux contribution of the α [curve (a)] and β phase [curve (b)] in the two-phase coexisting region to the total absorption flux [curve (c)], on the other hand, is much more balanced as Fig. 7(b) reveals. Again the maximum is found close to x_α.

Figure 8(a) shows the phase-normalized dissociation fluxes (reaction rates) in both phases. Again, the rate of hydrogen dissociation in the α phase is very low when the hydrogen concentration is small. At higher concentrations it increases and reaches the maximum near the phase-transition point x_α. In the two-phase region the dissociation rates remain constant, as expected. The hydrogen dissociation rateof the β-phase, on the other hand, is more or less constant in both the two-phase coexistence and β solid-solution region.

A similar behavior can be seen for the absorption rates in Fig. 8(b). Both rates are constant in the two-phase coexisting region and the β rate is substantially smaller than the α rate. The β rate declines quickly in the solid-solution region as the hydrogen concentration approaches its maximum. It is clear that both very large and very small hydrogen concentrations hinder the absorption kinetics. Obviously, it is difficult to absorb hydrogen into the bulk of the material if there are no host sites available anymore. Similarly, it is difficult to desorb hydrogen from the bulk if there is almost no hydrogen present. The same holds for the desorption kinetics as the absorption and desorption rates are equal under equilibrium conditions. So the subsurface kinetics is sensitive to extreme concentrations of hydrogen. This strongly contrasts to the present dissociation-recombination situation [Fig. 8(a)], where the rate in the β solid-solution range remains more or less constant.

Figure 9 shows the experimental pressure composition isotherms for all four (non)stoichiometric materials studied (symbols). Increasing the degree of non-stoichiometry induces the plateau pressures to increase. In addition, the plateaus are becoming much more sloping. The kinetic model perfectly fits (lines) the experimental results in all cases. In the case of $LaNi_{5.0}Cu_{1.0}$ [curve (d)], an $AB_{6.0}$ compound, an instantaneous phase transition has been adopted, in accordance with the reported experimental results.[3,25,26] The obtained parameter values are also given in Table I.

The good performance of the model is not restricted to the described model materials. Simulation of pressure composi-

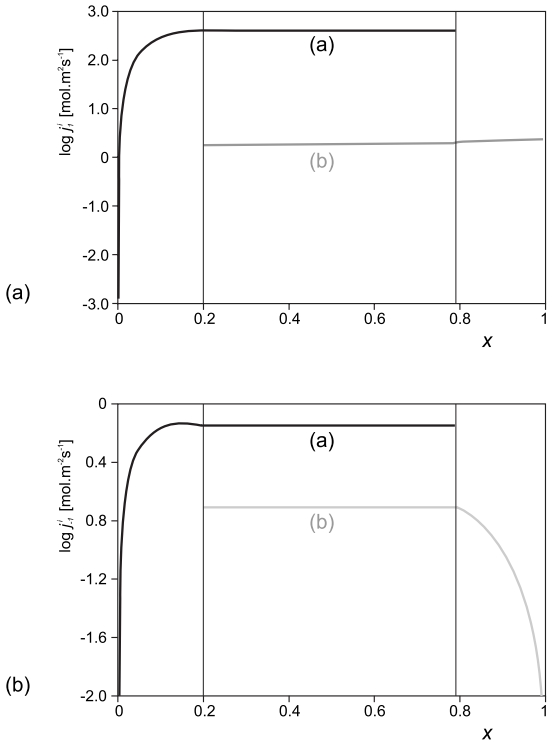

FIG. 8. (a) Phase-normalized dissociation fluxes (rates) at the α [curve (a)] and β phase [curve (b)] as a function of normalized hydrogen content (x) for $LaNi_{4.0}Cu_{1.0}$ under equilibrium conditions at 20 °C. (b) Phase-normalized absorption rates at the corresponding phases [curves (a) and (b)].

tion isotherms at various temperatures (0, 24, 45, 60, and 70 °C) of misch-metal-based, commercial, hydrogen storage materials[27,28] are shown in Fig. 10, curves (a)–(e), respectively. Again, the agreement between the simulations (lines) and experiments (symbols) is excellent over the entire hydrogen concentration range. As expected, the plateau pressure increases with increasing temperatures.

The calculations for the misch-metal-based materials were somewhat different from those employed for the AB_{5+x} materials. The 24 °C sample [curve (a)] was calculated in the same way as all AB_{5+x} alloys, i.e., P_α was set to normal

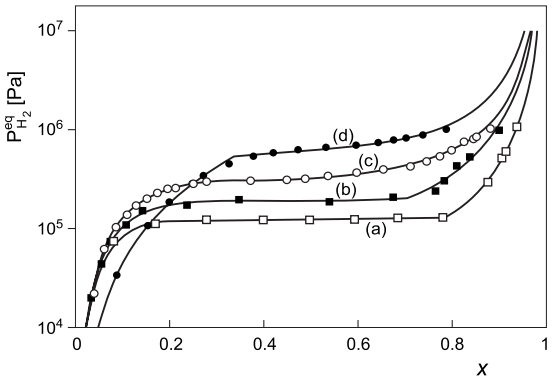

FIG. 9. Measured (symbols) and calculated (lines) pressure-composition isotherms for various (non)stoichiometric compounds: $LaNi_{4.0}Cu_{1.0}$ (a), $LaNi_{4.2}Cu_{1.0}$ (b), $LaNi_{4.4}Cu_{1.0}$ (c), $LaNi_{5.0}Cu_{1.0}$ (d). All measurements have been performed via the gas phase at 20 °C (Refs. 3, 25, and 26).

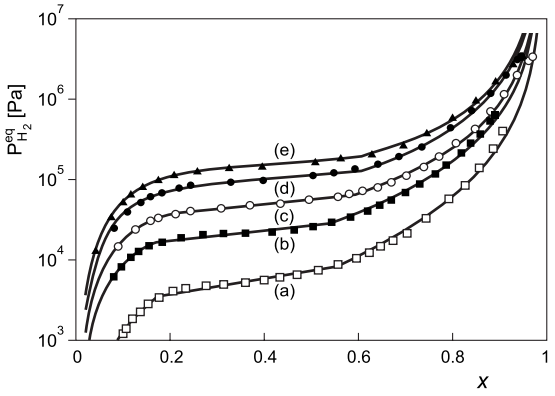

FIG. 10. Measured (symbols) and calculated (lines) pressure-composition isotherms for commercial, misch-metal-based, AB_5-type hydrogen storage materials at 0 (a), 24 (b), 45 (c) 60 (d), and 70 °C (e) (Refs. 27 and 28).

atmospheric pressure (10^5 Pa). For the other temperatures this parameter was considered a variable, because with a fixed P_α the fits were found to be poor. All obtained values of the model parameters are listed in Table II. The calculated energies are all in a physically meaningful range and reveal a similar behavior as found in the LGM simulations.[13] The difference in calculated values between the LGM and kinetic model is minor with only one exception: due to different continuity conditions [Eqs. (49) and (50)] the values of parameter L are of opposite signs compared with those obtained from the LGM. However, it has only a limited impact since the absolute values of L are one-to-two orders of magnitude smaller than the other energy related parameters.

The simulation results of hydride-forming materials can now be represented in various forms, revealing the strength of the present model. For example, for some applications it is interesting to see how the hydrogen concentration inside the alloy changes with temperature when the equilibrium hydrogen pressure is kept constant, i.e., under isobaric conditions. Figure 11 illustrates these dependencies where the solid lines, the simulated isobars, are based on the presented model and parameters in Table II, and the data points are experimentally observed. Curves (a), (b), (c), and (d) correspond to equilibrium hydrogen pressures of 10^4, 2×10^4, 4×10^4, and 8×10^4 Pa, respectively. As expected, the normalized hydrogen concentration decreases with increasing temperature.[1] However this decrease is not monotonically uniform. Each curve reveals a steep region in which the hydrogen concentration increases sharply with temperature. At the left and at the right of those regions the isobars are relatively flat. It is interesting to point out that a significant increase in the amount of stored hydrogen (~2–3 times) may be achieved by a relatively small decrease in temperature of about 10 °C. This indicates that the isobaric hydrogen storage process is highly temperature efficient for this material.

The principles outlined in this publication are not only restricted to hydrogen storage of the AB_5 type but can obviously also be applied to other crystallographic host materials such as, for example, AB_2, AB, and A_2B hydride-forming compounds.[1,27] It should be noted that when phase-transitions are not isomorphological, d^b [Eq. (4)] might de-

viate from unity and mathematical derivations become more complex. Evidently, the model can also be easily expanded when more than one phase transition is involved. In the forthcoming paper the nonequilibrium gas phase conditions will be addressed and, in addition, electrochemical hydrogen storage will be considered.

IV. CONCLUSIONS

A kinetic model has been proposed, describing hydrogen storage in hydride-forming materials under equilibrium conditions. The model is based on first principles of chemical reaction kinetics, statistical thermodynamics and includes structural changes induced by (de)hydrogenation. It takes into account forward reactions of dissociation of hydrogen gas molecules at the material surface and hydrogen absorption into the bulk of the hydride-forming material and backward processes of hydrogen desorption and recombination.

The fluxes of the dissociation and recombination reactions and those of the absorption and desorption reactions are considered equal under equilibrium conditions, which yields expressions for hydrogen concentrations in different areas of the system. Elegantly, the kinetic model makes use of the previously described lattice gas model and includes thermodynamically derived parameters from the introduced "rectangular rule," making it much more physically transparent. A complete set of equations, describing pressure-composition isotherms, including phase transformation has been obtained.

The equilibrium pressure is defined in terms of the normalized surface coverage θ and normalized hydrogen concentration x, using parameters, such as phase-transition points, interaction energies between hydrogen atoms, and host energies of the crystal structure of the material. The final set of equilibrium pressure equations consists of three parts: for $x<x_\alpha$ and $x>x_\beta$ solid-solution regions are obtained for the α and β phase, respectively, which are characterized by a logarithmic form; for $x_\alpha<x<x_\beta$, a more complex equation accurately describes the two-phase coexistence region.

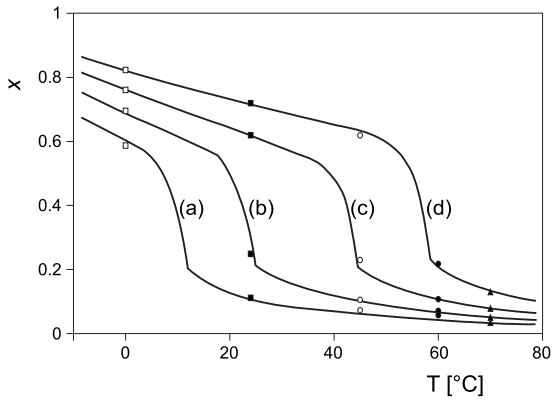

FIG. 11. Isobars for commercial, misch-metal-based, AB_5-type hydrogen storage materials at equilibrium pressures of 10^4 (a), 2×10^4 (b), 4×10^4 (c), and 8×10^4 Pa (d). The lines are based on the calculations using the parameter values given in Table II. Data points are experimentally observed (symbols correspond also to Fig. 10).

TABLE II. Simulated parameter values under equilibrium kinetic conditions for commercial, misch-metal-based, AB_5-type materials at various temperatures. Bold parameters are obtained by optimization.

N	Par	Dimension	0 °C	24 °C	45 °C	60 °C	70 °C
1	x_α	[a]	0.184	0.211	0.208	0.235	0.229
2	x_β	[a]	0.581	0.556	0.596	0.603	0.603
3	E^b_α	eV	**0.009**	0.037[a]	**0.045**	**0.052**	**0.056**
4	E^b_β	eV	**0.004**	**0.027**	**0.046**	**0.053**	**0.065**
5	$U^b_{\alpha\alpha}$	eV[a]	−0.046	−0.115	−0.123	−0.125	−0.128
6	$U^b_{\beta\beta}$	eV[a]	−0.007	−0.025	−0.045	−0.051	−0.064
7	$U^b_{\alpha\beta}$	eV[b]	−0.036	−0.109	−0.170	−0.179	−0.216
8	L	eV[b]	-0.312×10^{-3}	-1.257×10^{-3}	-5.110×10^{-3}	-5.659×10^{-3}	-8.128×10^{-3}
9	B_1^α	[b]	0.442×10^3	0.508×10^3	0.644×10^3	0.853×10^3	1.013×10^3
10	B_1^β	[b]	24.44	32.22	33.47	51.71	55.34
11	B_2^α	[c]	1	1	1	1	1
12	B_2^β	[c]	1	1	1	1	1
13	P_α	Pa	$\mathbf{0.824}\times10^5$	10^5[c]	$\mathbf{1.397}\times10^5$	$\mathbf{1.918}\times10^5$	$\mathbf{2.371}\times10^5$
14	P_β	Pa	$\mathbf{4.55}\times\mathbf{10}^3$	$\mathbf{6.53}\times\mathbf{10}^3$	$\mathbf{7.47}\times\mathbf{10}^3$	$\mathbf{11.96}\times\mathbf{10}^3$	$\mathbf{13.32}\times\mathbf{10}^3$
15	E^s_α	eV[b]	0	0	0	0	0
16	E^s_β	eV[b]	0	0	0	0	0
17	$U^s_{\alpha\alpha}$	eV[b]	0	0	0	0	0
18	$U^s_{\beta\beta}$	eV[b]	0	0	0	0	0

[a]Parameters are taken from the lattice gas model (Ref. 13).
[b]Parameters are calculated from the continuity conditions.
[c]Parameters are set constant by normalization.

Simulations of experimental absorption isotherms have been presented for both model AB_{5+x}-type and commercial AB_5-type misch-metal-based materials. The calculated pressure-composition isotherms show excellent agreement with the experimentally obtained results in all cases. Moreover, the transparent model presented in the present paper gives a detailed insight into the various flux- and surface dependencies on the hydrogen content. The model has been applied to simulate the isobaric conditions. It has been concluded that for misch-metal-based hydrogen storage alloys the isobaric process is highly temperature efficient.

After detailed analyses of the hydrogen storage kinetics of the investigated materials, it can be concluded that the dissociation/recombination kinetics at the α phase is, in general, faster than those at the β phase. In addition, it was found that the hydrogen reaction kinetics is very sensitive to both extremely low and high hydrogen concentrations.

*Author to whom correspondence should be addressed; Peter.Notten@Philips.com

[1] Y. Fukai, *The Metal-Hydrogen System* (Springer-Verlag, Berlin, 1993).
[2] T. B. Flanagan, *Thermodynamics of Metal-gas Reactions* (Kluwer, Dordrecht, 1995), p. 43.
[3] P. H. L. Notten, *Interstitial Intermetallic Alloys*, edited by F. Grandjean, G. J. Long, and K. H. J. Buschow, Vol. 281 of NATO Advanced Studies Institute, Series E: Applied Sciences (Plenum, New York, 1995), Chap. 7.
[4] P. H. L. Notten and M. Latroche, *Nickel-MetalHydride Batteries: A Successful Application of Hydrogen Storage Materials* (Encyclopedia of Electrochemical Power Sources, in press).
[5] L. Schlapbach and A. Zuttel, Nature (London) **414**, 353 (2002).
[6] K. H. J. Buschov, P. C. P. Bouten, and A. R. Miedema, Rep. Prog. Phys. **45**, 937 (1982).
[7] R. Griessen and T. Riesterer, *Heat Formation Models*, edited by L. Schlapbach, Topics in Applied Physics (Springer-Verlag, Berlin, 1988), p. 219.
[8] L. Schlapbach, *Surface Properties and Activation*, edited by L. Schlapbach, Topics in Applied Physics (Springer-Verlag, Berlin, 1992), p. 15.
[9] H. Frieske and E. Wicke, Ber. Bunsenges. Phys. Chem. **77**, 48 (1973).
[10] Y. Sakamoto, E. Kakihisa, and Y. Kinari, Z. Phys. Chem. **179**, 69 (1993).
[11] A. Ledovskikh, E. Verbitskiy, A. Ayeb, and P. H. L. Notten, J. Alloys Compd. **356-357**, 742 (2003).
[12] T. B. Flanagan and W. A. Oates, Top. Appl. Phys. **63**, 49 (1988).
[13] A. Ledovskikh, D. Danilov, W. J. J. Rey, and P. H. L. Notten, Phys. Rev. B, **73**, 014106 (2006).
[14] M. Martin, C. Gommel, C. Borkhart, and E. Fromm, J. Alloys Compd. **238**, 193 (1996).
[15] G. E. Fernandez, D. Rodriguez, and G. Meyer, Int. J. Hydrogen Energy **23**, 1193 (1998).
[16] E. P. Feldman, A. D. Alexeev, T. N. Melnik, and L. N. Gurmen, Int. J. Hydrogen Energy **30**, 509 (2005).
[17] E. Gileadi and B. E. Conway, in *Modern Aspects of Electrochemistry*, edited by J. O'M. Bockris and B. E. Conway (Butterworth, London, 1964)
[18] E. Gileadi, in *Electrosorption*, edited by E. Gileadi (Plenum, New York, 1967), Chap. 1.
[19] F. Feng, M. Geng, and D. O. Northwood, Comput. Mater. Sci. **23**, 291 (2002).
[20] S. E. Millman and G. Kirczenow, Phys. Rev. B **28**, 3482 (1983).
[21] S. A. Safran, Phys. Rev. Lett. **44**, 937 (1980).
[22] T. L. Hill, *An Introduction to Statistical Thermodynamics* (Addison-Wesley, New York, 1960).
[23] W. R. McKinnon and R. R. Haering, *Physical Mechanism of Intercalation* (National Resource Council Canada, Ottawa, 1983), p. 235.
[24] R. Kubo, *Thermodynamics: An Advanced Course with Problems and Solutions* (North Holland, Amsterdam, 1968).
[25] P. H. L. Notten, R. E. F. Einerhand, and J. L. C. Daams, J. Alloys Compd. **210**, 221 (1994).
[26] P. H. L. Notten, J. L. C. Daams, and R. E. F. Einerhand, J. Alloys Compd. **210**, 233 (1994).
[27] H. Senoh, K. Morimoto, H. Inoue. C. Iwakura, and P. H. L. Notten, J. Electrochem. Soc. **147**, 2451 (2000).
[28] Y. Dansui and P. H. L. Notten (private communications).